Rotational mode specificity in the Cl + CHD3 HCl + CD3 reaction

Rui Liu, Fengyan Wang, Bin Jiang, Gábor Czakó, Minghui Yang, Kopin Liu, and Hua Guo

Citation: The Journal of Chemical Physics **141**, 074310 (2014); doi: 10.1063/1.4892598
View online: http://dx.doi.org/10.1063/1.4892598
View Table of Contents: http://scitation.aip.org/content/aip/journal/jcp/141/7?ver=pdfcov
Published by the AIP Publishing

Rotational mode specificity in the Cl + CHD_3 → HCl + CD_3 reaction

Rui Liu,[1] Fengyan Wang,[2,3,a)] Bin Jiang,[4] Gábor Czakó,[5,a)] Minghui Yang,[1,a)] Kopin Liu,[2,a)] and Hua Guo[4,a)]

[1]*Key Laboratory of Magnetic Resonance in Biological Systems, Wuhan Center for Magnetic Resonance, State Key Laboratory of Magnetic Resonance and Atomic and Molecular Physics, Wuhan Institute of Physics and Mathematics, Chinese Academy of Sciences, Wuhan 430071, China*
[2]*Institute of Atomic and Molecular Sciences, Academia Sinica, Taipei 10617, Taiwan*
[3]*Department of Chemistry, Fudan University, Shanghai 200433, China*
[4]*Department of Chemistry and Chemical Biology, University of New Mexico, Albuquerque, New Mexico 87131, USA*
[5]*Laboratory of Molecular Structure and Dynamics, Institute of Chemistry, Eötvös University, P.O. Box 32, H-1518, Budapest 112, Hungary*

(Received 10 July 2014; accepted 29 July 2014; published online 18 August 2014)

By exciting the rotational modes of vibrationally excited $CHD_3(v_1 = 1, JK)$, the reactivity for the Cl + CHD_3 → HCl + CD_3 reaction is observed enhanced by as much as a factor of two relative to the rotationless reactant. To understand the mode specificity, the reaction dynamics was studied using both a reduced-dimensional quantum dynamical model and the conventional quasi-classical trajectory method, both of which reproduced qualitatively the measured enhancements. The mechanism of enhancement was analyzed using a Franck-Condon model and by inspecting trajectories. It is shown that the higher reactivity for higher J states of CHD_3 with $K = 0$ can be attributed to the enlargement of the cone of acceptance. On the other hand, the less pronounced enhancement for the higher $J = K$ states is apparently due to the fact that the rotation along the C–H bond is less effective in opening up the cone of acceptance. © *2014 AIP Publishing LLC*. [http://dx.doi.org/10.1063/1.4892598]

I. INTRODUCTION

Thanks to numerous experimental and theoretical studies, it is now well established that all forms of energy are not equal in promoting reactivity, particularly for gas phase and gas-surface bimolecular reactions.[1–3] The mode specificity and related bond selectivity are of great importance not only for a better understanding of reaction dynamics but may also have practical implications as a single reactant quantum state can nowadays be readily prepared by laser.[4]

The accumulation of experimental and theoretical evidence has allowed the distillation of general principles and rules governing mode specificity. Polanyi has, for example, proposed a set of intuitive and powerful rules for predicting the relative efficacies of the reactant vibrational and translational excitations in atom-diatom reactions.[5] For a reaction with a reactant-like or early barrier, the translational energy is more effective in surmounting the barrier. For a reaction with a product-like or late barrier, on the other hand, vibrational energy has a higher efficacy in promoting the reaction. Recently, Polanyi's rules have been extensively tested in reactions involving polyatomic molecules both experimentally[6–13] and theoretically.[14–23] These studies have stimulated several new models to understand the energy flow and mode specificity in polyatomic reactions.[21,24,25]

Despite the tremendous progress, there have been very few experimental studies on the effect of reactant rotation on reactivity at a quantum state resolved level.[26–28] On the other hand, there were many theoretical studies of the rotational effect,[29–40] although few were concerned with rotation of polyatomic reactants.[41–45] Since the energy gap between rotational states is typically much smaller than that for vibration, the impact of rotational excitation is often greater per unit energy than its vibrational counterpart. In this publication, we demonstrate a rotational effect for the title reaction pronounced on the per unit energy basis and provide theoretical analysis of the mode specificity.

II. METHODS

A. Experimental method

The crossed molecular-beam experiment is essentially the same as the previous reports.[11,13] The Cl-beam was generated by pulsed-discharging a mixture of 5% Cl_2 in Ne at a pulsed-valve pressure of 5 atm. A seeded beam of 30% CHD_3 in He (5 atm) was then crossed with the Cl-atom beam in a source-rotatable vacuum chamber. The CH stretch-excited $CHD_3(v_1 = 1)$ reactants were prepared by an infrared (IR) optical parametric oscillator/amplifier (OPO/A) in the source chamber through a multipass ring reflector.[12,46] Since the IR-excited reactants have to travel about 100 μs before reaching the collisional zone, any initial alignment upon IR excitation will be lost due to the hyperfine depolarization effects,[47–50] and thus the rovibrationally excited methane is unpolarized in this work. Several rotational branches of the $CHD_3(v_1 = 1 \leftarrow 0)$ transition were exploited to prepare the lowest few rotational states of $CHD_3(v_1 = 1)$. To determine the rotationally state-selected reactivity of the Cl + $CHD_3(v_1 = 1, JK)$

a)Authors to whom correspondence should be addressed. Electronic addresses: fengyanwang@fudan.edu.cn; czako@chem.elte.hu; yangmh@wipm.ac.cn; kliu@pub.iams.sinica.edu.tw; and hguo@unm.edu

reaction, one needs to know the fraction of reactants, $n^{\neq}/n_0$, being excited and contributing to the observed product signals. We employed the depletion method,[12] i.e., the IR-induced signal depletion in the F + $CHD_3(v_1 = 1,JK)$ → $CHD_2(v = 0)$ + DF reaction, to quantify such quantities. The depletion measurements were performed before and after each experiment to ensure consistency. The resultant $n^{\neq}/n_0$ for the R(1), Q(1), R(0), and P(1) branches are 0.29, 0.19, 0.12, and 0.045, respectively.[51] Within the experimental errors (typically 0.015), these values are independent of the collision energy (E_c) in this study.

The vibrational ground state of CD_3 products in the Cl + $CHD_3(v_1 = 1,JK)$ reaction was detected by a (2+1) resonance-enhanced multiphoton ionization (REMPI) process of the $CD_3(0_0^0)$ band[52–54] and measured by a time-sliced velocity imaging technique.[55] The full rotational state distribution of $CD_3(v = 0)$ was sampled in this study by scanning the probe laser frequency back and forth over the Q-head spectral profile while the image was acquired.[13] The product images were recorded in an alternating IR-on and IR-off manner. Each recorded image comprised three spectral scans, and the pair of on/off images was repeated 25–130 times for improving signal-to-noise ratios. After the density-to-flux correction to the recorded images[55,56] and with the knowledge of $n^{\neq}/n_0$, the desired product speed and state-resolved angular distributions, as well as the relative reactivity of initially selected rotation states of CHD_3 can be deduced.[13,57] Only the relative reactivity, i.e., the sum of both HCl($v = 0$) and HCl($v = 1$) correlated to the $CD_3(v = 0)$ products, is presented here for theoretical comparisons. The more detailed product distributions will be reported in the future.

B. Reduced-dimensional quantum mechanical method

The Cl + CHD_3 reaction is approximately treated with the seven-dimensional (7D) Palma-Clary model for the X + CYZ_3 system, in which the CZ_3 moiety is assumed to maintain its C_{3v} symmetry throughout.[58–60] In this reduced-dimensional quantum dynamics (QD) model, the Jacobi coordinates shown in Fig. 1 were employed, in which $\boldsymbol{R}$ is the vector from the center of mass of CYZ_3 to X; $\boldsymbol{r}$ is the vector from the center of mass of CZ_3 to Y; q is the CZ bond length fixed at the value of 2.067 a.u.; χ is the angle between a CZ bond and the symmetry axis, vector $\boldsymbol{s}$, of CZ_3. To describe the angular coordinates and rotation of the system, it is useful to introduce four frames, namely, the space-fixed frame, the body-fixed frame ($XCYZ_3$-fixed frame), the CYZ_3-fixed frame, and the CZ_3-fixed frame. The z-axis of the body-fixed frame lies along the vector $\boldsymbol{R}$ and the vector $\boldsymbol{r}$ is always in the xz-plane of the frame. The z-axis of the CYZ_3-fixed frame lies along the vector $\boldsymbol{r}$ and the vector $\boldsymbol{s}$ is always in the xz-plane of the frame. The z-axis of the CZ_3-fixed frame lies along its symmetry axis, vector $\boldsymbol{s}$, and the first Z atom is always in the xz-plane of the frame. The four frames form three pairs of related space and body-fixed frames. We define the bending angle between vectors $\boldsymbol{R}$ and $\boldsymbol{r}$ to be θ_1; φ_1 is the azimuth angle of the rotation of CYZ_3 around the vector $\boldsymbol{r}$; θ_2 is the bending angle between vectors $\boldsymbol{r}$ and $\boldsymbol{s}$; and φ_2 is the azimuth angle of the rotation of CZ_3 around vector $\boldsymbol{s}$.

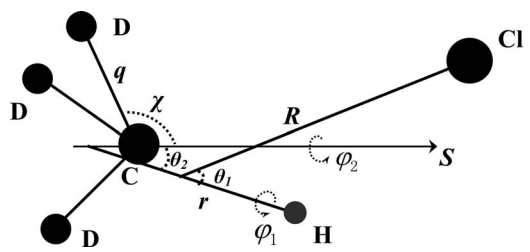

FIG. 1. The coordinate system used in the quantum dynamics calculations.

The model Hamiltonian for the X + CYZ_3 system is given by ($\hbar = 1$)[58,59]

$$\hat{H} = -\frac{1}{2\mu_R}\frac{\partial^2}{\partial R^2} - \frac{1}{2\mu_r}\frac{\partial^2}{\partial r^2} + \frac{(\hat{J}_{tot} - \hat{J})^2}{2\mu_R R^2} + \frac{\hat{l}^2}{2\mu_r r^2} + \hat{K}^{vib}_{CZ_3} + \hat{K}^{rot}_{CZ_3} + V(R, r, \chi, \theta_1, \varphi_1, \theta_2, \varphi_2), \quad (1)$$

where μ_R and μ_r are the reduced masses for R and r, respectively. $\hat{J}_{tot}$ is the total angular momentum operator of the system; $\hat{J}$ is the rotational angular momentum operator of CYZ_3; and $\hat{l}$ is the orbital angular momentum operator of atom Y with respect to CZ_3. $\hat{K}^{vib}_{CZ_3}$ and $\hat{K}^{rot}_{CZ_3}$ are the vibrational and rotational kinetic energy operators of CYZ_3, respectively:

$$\hat{K}^{vib}_{CZ_3} = -\frac{1}{2q^2}\left(\frac{\cos^2\chi}{\mu_x} + \frac{\sin^2\chi}{\mu_s}\right)\frac{\partial^2}{\partial\chi^2} - \frac{1}{q^2}\sin\chi\cos\chi\frac{\partial}{\partial\chi} \quad (2)$$

and

$$\hat{K}^{rot}_{CZ_3} = \frac{1}{2I_A}\hat{j}^2 + \left(\frac{1}{2I_C} - \frac{1}{2I_A}\right)\hat{j}_z^2, \quad (3)$$

where μ_x and μ_s are related to the mass of atoms C and Z, $\mu_x = 3m_Z$, and $\mu_s = 3m_C m_Z/(m_C + 3m_Z)$. I_A and I_C are the moments of inertia of CZ_3, defined as

$$I_A = \frac{3}{2}m_Z q^2\left(\sin^2\chi + \frac{2m_C}{m_C + 3m_Z}\cos^2\chi\right), \quad (4)$$

$$I_C = 3m_Z q^2\sin^2\chi. \quad (5)$$

$\hat{j}$ is the rotational angular momentum of CZ_3 with $\hat{j}_z$ as its z-component. No vibration-rotation coupling exists due to the symmetry requirement and the definition of the CZ_3-fixed frame. Finally, the last term in Eq. (1) represents the potential energy surface (PES), which is developed by Czakó and Bowman.[17,61]

According to the definition of the four frames above, the rotational basis functions for the $XCYZ_3$ system can be written as

$$\Phi^{J_{tot}M_{tot}K_{tot}}_{Jjlk}(\hat{R}, \hat{r}, \hat{s}) = \bar{D}^{J_{tot}}_{M_{tot}K_{tot}}(\hat{R})Y^{JK_{tot}}_{jlk}(\hat{r}, \hat{s}), \quad (6)$$

where the $\bar{D}^{J_{tot}}_{M_{tot}K_{tot}}(\hat{R})$ is defined as

$$\bar{D}^{J_{tot}}_{M_{tot}K_{tot}}(\hat{R}) = \sqrt{\frac{2J+1}{8\pi^2}}D^{*J_{tot}}_{M_{tot}K_{tot}}(\alpha, \beta, \gamma), \quad (7)$$

and M_{tot} and K_{tot} are the projection of total angular momentum J_{tot} on the z-axis of the space-fixed and body-fixed

frames, respectively, and $D^{J_{tot}}_{M_{tot}K_{tot}}$ is the Wigner rotational matrix.[62] $\bar{D}^{J_{tot}}_{M_{tot}K_{tot}}(\hat{R})$ depends on the three Euler angles which rotate the space-fixed frame onto the body-fixed frame and are the eigenfunctions of $\hat{J}^2_{tot}$. The spherical harmonics are given by

$$Y^{JK_{tot}}_{jlk}(\hat{r},\hat{s}) = \sum_K \bar{D}^J_{K_{tot}K}(\hat{r})\sqrt{\frac{2l+1}{2J+1}}\langle jKl0|JK\rangle \bar{D}^j_{Kk}(\hat{s}), \tag{8}$$

where $\bar{D}^J_{K_{tot}K}(\hat{r})$ depends on the three Euler angles which rotate the $XCYZ_3$ body-fixed frame onto the CYZ_3-fixed frame and $\bar{D}^j_{Kk}(\hat{s})$ depends on the three Euler angles which rotate the CYZ_3-fixed frame onto the CZ_3-fixed frame,

$$\bar{D}^J_{K_{tot}K}(\hat{r}) = \sqrt{\frac{2J+1}{4\pi}} D^{*J}_{K_{tot}K}(0,\theta_1,\varphi_1), \tag{9}$$

$$\bar{D}^j_{Kk}(\hat{s}) = \sqrt{\frac{2j+1}{4\pi}} D^{*j}_{Kk}(0,\theta_2,\varphi_2). \tag{10}$$

The parity-adapted rotational basis function should be a linear combination of $\Phi^{J_{tot}M_{tot}K_{tot}}_{Jljk}$ and $\Phi^{J_{tot}M_{tot}-K_{tot}}_{Jlj-k}$,

$$\begin{aligned}\Phi^{J_{tot}M_{tot}\bar{K}_{tot}\varepsilon}_{Jljk}(\hat{R},\hat{r},\hat{s}) &= \sqrt{\frac{1}{2(1+\delta_{\bar{K}0}\delta_{k0})}} \\ &\times \left[\Phi^{J_{tot}M_{tot}\bar{K}_{tot}}_{Jljk}(\hat{R},\hat{r},\hat{s}) + \varepsilon(-1)^{J_{tot}+J+l+j+k}\right. \\ &\left.\times \Phi^{J_{tot}M_{tot}-\bar{K}_{tot}}_{Jlj-k}(\hat{R},\hat{r},\hat{s})\right],\end{aligned} \tag{11}$$

where $\bar{K}_{tot} = |K_{tot}|$.

The time-dependent wavefunction is expanded in the parity-adapted rotational basis functions as

$$\begin{aligned}\Psi^{J_{tot}M_{tot}\varepsilon} = \sum_{n_R,n_r,n_u}\sum_{K_{tot}Jljk} & c^{J_{tot}M_{tot}K_{tot}\varepsilon}_{n_Rn_rn_uJljk}(t) G_{n_R}(R) F_{n_r}(r) \\ & \times H_{n_u}(\chi)\Phi^{J_{tot}M_{tot}K_{tot}\varepsilon}_{Jljk}(\hat{R},\hat{r},\hat{s}),\end{aligned} \tag{12}$$

where $c^{J_{tot}M_{tot}K_{tot}\varepsilon}_{n_Rn_rn_uJljk}(t)$ are time-dependent coefficients. n_R, n_r, and n_χ are labels for the basis functions in R, r, and χ, respectively. $G_{n_R}(R)$ are sine basis functions.[63] The basis functions $F_{n_r}(r)$ and $H_{n_u}(\chi)$ are obtained by solving one-dimensional reference Hamiltonians, defined as follows:

$$\hat{h}_r(r) = -\frac{1}{2\mu_r}\frac{\partial^2}{\partial r^2} + v^{ref}_r(r), \tag{13}$$

$$\hat{h}_u(\chi) = \hat{K}^{vib}_{CZ_3} + v^{ref}_u(\chi), \tag{14}$$

where $v^{ref}_r(r)$ and $v^{ref}_u(\chi)$ are the corresponding reference potentials.

The initial state wavefunction for the specific state (J_{tot}, M_{tot}, ε) of the system is constructed as the direct product of a localized wavepacket for $G^0(R)$, the rotation matrix $\bar{D}^{J_{tot}}_{M_{tot}K_{tot}}(\hat{R})$, and the eigenfunction of CYZ_3 of the specific state (n_0, J_0, K_0, p_0), where n_0, J_0, K_0, and p_0 represent, respectively, the initial vibrational quantum number, the rotational index (JK), and the parity of the symmetric rotor CYZ_3.

In general, $G^0(R)$ is chosen to be a Gaussian function,

$$G^0(R) = (\pi\delta^2)^{-1/4}\exp\left(-\frac{(R-R_0)^2}{2\delta^2}\right)\exp(-i\kappa_0 R), \tag{15}$$

where R_0 and δ are the center and width of the Gaussian function; $\kappa_0 = \sqrt{2\mu_R E_0}$ and E_0 is the central energy of the Gaussian function.

The rovibrational eigenfunction of CYZ_3, $\psi^{J_{tot}M_{tot}\varepsilon}_{n_0J_0K_0p_0}$, is expanded as

$$\psi^{J_{tot}M_{tot}\varepsilon}_{n_0J_0K_0p_0} = \sum_{n_rn_uljk} d^{n_0J_0K_0p_0}_{n_rn_uljk} F_{n_r}(r) H_{n_u}(\chi)\Phi^{J_{tot}M_{tot}\bar{K}_0\varepsilon}_{J_0ljk}(\hat{R},\hat{r},\hat{s}), \tag{16}$$

which is an eigenfunction of the following Hamiltonian:

$$\begin{aligned}\hat{H}_{YCZ_3} = & -\frac{1}{2\mu_r}\frac{\partial^2}{\partial r^2} + \frac{\hat{l}^2}{2\mu_r r^2} \\ & + \hat{K}^{vib}_{CZ_3} + \hat{K}^{rot}_{CZ_3} + V_{YCZ_3}(r,\chi,\theta_2,\varphi_2),\end{aligned} \tag{17}$$

where the potential used here is $V_{YCZ_3}(r,\chi,\theta_2,\varphi_2) = V(R = \infty, r, \chi, \theta_1, \theta_2, \varphi_1, \varphi_2)$.

The wavefunction was propagated using the split-operator propagator,[64]

$$\Psi(t+\Delta) = e^{-i\hat{H}_0\Delta/2}e^{-iU\Delta}e^{-i\hat{H}_0\Delta/2}\Psi(t), \tag{18}$$

where the reference Hamiltonian $\hat{H}_0$ is defined as

$$\hat{H}_0 = -\frac{1}{2\mu_R}\frac{\partial^2}{\partial R^2} + \hat{h}^{ref}_r(r) + \hat{h}^{ref}_u(\chi), \tag{19}$$

and the reference potential U is defined as

$$\begin{aligned}U = & \frac{(\hat{J}_{tot}-\hat{J})^2}{2\mu_R R^2} + \frac{\hat{l}^2}{2\mu_r r^2} + \hat{K}^{rot}_{CZ_3} \\ & + V(R,r,\chi,\theta_1,\varphi_1,\theta_2,\varphi_2) - v^{ref}_r(r) - v^{ref}_u(\chi).\end{aligned} \tag{20}$$

The total reaction probabilities for the specific initial state for a whole energy range can be calculated from the time-independent wavefunction at a dividing surface $r = r_s$,

$$P_i(E) = \frac{1}{\mu_r}\mathrm{Im}(\langle\psi_{iE}|\psi'_{iE}\rangle)|_{r=r_s}, \tag{21}$$

where ψ_{iE} and ψ'_{iE} are the time-independent wavefunction and its first derivative in r. The time-independent wavefunction ψ_{iE} was constructed by a Fourier transformation of the time-dependent wavepacket as follows:

$$|\psi_{iE}\rangle = \frac{1}{a_i(E)}\int_0^\infty e^{iEt}|\Psi_i(t)\rangle dt. \tag{22}$$

The coefficient $a_i(E)$ is the overlap between the initial wavepacket $\Psi_i(0)$ and the energy-normalized asymptotic scattering function ϕ_{iE}, $a_i(E) = \langle\phi_{iE}|\Psi_i(0)\rangle$.

Finally, the total reaction integral cross section is computed by summing up the partial waves:

$$\sigma_{J,K,K_{tot}}(E_c) = \frac{1}{2J+1}\frac{\pi}{2\mu_R E_c}\sum_{J_{tot}=0}^{\infty}(2J_{tot}+1)P^{J_{tot}}_{J,K,K_{tot}}(E_c). \quad (23)$$

Since the exact close-coupling calculations for $J_{tot} > 0$ state are too expensive computationally, the centrifugal-sudden (CS) approximation[65,66] within a body-fixed (BF) representation was employed in the calculations for $J_{tot} > 0$. In addition to J_{tot}, the projection of total angular momentum on the BF axis, K_{tot}, is also a good quantum number within the CS limit. K_{tot} is also the projection of reactant HCD_3 angular momentum (J) on the BF z-axis $\boldsymbol{R}$, and thus there are $(2J + 1)$ allowed values for K_{tot}: $-J, -J + 1, \ldots, J$. The CS Hamiltonian depends only on K^2_{tot} and it suffices to take $K_{tot} = 0, 1, 2, \ldots, J$, and weight any probabilities for $K > 0$ by 2.

$$\sigma_{J,K}(E_c) = \sigma_{J,K,0}(E_c) + 2\sum_{K_{tot}=0}^{\min(J,J_{tot})}\sigma_{J,K,K_{tot}}(E_c). \quad (24)$$

An L-shaped wavefunction expansion for R and r was used to reduce the size of the basis set.[67] A total of 240 sine basis functions ranging from 3.0 to 15.0 bohrs were used for the R basis set expansion with 100 nodes in the interaction region; and 5 and 25 basis functions of r were used in the asymptotic and interaction regions, respectively. For the umbrella motion 12 basis functions were used. The size of the rotational basis functions is controlled by the parameters, $J_{\max} = 57$, $l_{\max} = 33$, $j_{\max} = 24$, and $k_{\max} = 9$. After considering parity and C_{3v} symmetry, the size of rotational basis functions was 52 634–232 880 and the size of the total basis functions was 2.0×10^9–8.9×10^9, depending on J_{tot} and the A/E symmetry of CD_3 rotation around its C_{3v} axis. The number of nodes for the integration of the rotational basis set was 253 750 and the total number of nodes was 11×10^9. The center of the Gaussian wavepacket was located at $R_0 = 13.0$ bohrs. The width of wavepacket $\delta = 0.06$ bohr and the central energy of the Gaussian wavepacket was $E_0 = 0.3$ eV. The vibrational states of CHD_3 for the total angular momentum of CHD_3 $J = 0, 1, 2$ were solved using the basis set above. The maximum value of J_{tot} needed to converge the integral cross section is $J_{tot} = 147$.

C. Quasi-classical trajectory method

Quasi-classical trajectory (QCT) calculations for the $Cl(^2P_{3/2}) + CHD_3(v_1 = 1, JK) \rightarrow HCl + CD_3$ reaction were performed using the same full-dimensional spin-orbit-corrected PES developed by Czakó and Bowman.[17,61] We employed standard normal mode sampling[68] to prepare the quasi-classical CH stretching-excited state ($v_1 = 1$) of CHD_3. The initial rotational quantum numbers JK were set by following the procedure described in Ref. 68. In brief, the three components (J_x, J_y, J_z) of the classical angular momentum vector $\boldsymbol{J}$ are sampled in the principal axis system, where J_z is set to K and J_x and J_y are sampled randomly, while the length of $\boldsymbol{J}$ is $[J(J + 1)]^{1/2}$. Then, $\boldsymbol{J}$ is transformed to the space fixed frame and standard modifications of the velocities are done to set the desired $\boldsymbol{J}$.[68]

The initial distance of the Cl atom from the center of the mass of CHD_3 was $\sqrt{x^2 + b^2}$, where b is the impact parameter and x was set to 10 bohrs. The orientation of CHD_3 was randomly sampled and b was scanned from 0 to 7 bohrs with a step size of 1.0 bohr. Five thousand trajectories were computed at each b; thus, the total number of trajectories was 40 000 for each E_c and JK. We have run QCTs at several collision energies in the 1−10 kcal/mol range. All the trajectories were integrated using 0.0726 fs integration step allowing a maximum of 20 000 time steps (∼1.5 ps). (Most of the trajectories finished much faster, i.e., within a few hundred fs.) The trajectories were analyzed without a zero-point energy constraint.

The integral cross section for the title reaction was calculated according to the following formula:

$$\sigma = \pi\sum_{n=1}^{n_{\max}}[b_n - b_{n-1}][b_n P(b_n) + b_{n-1}P(b_{n-1})], \quad (25)$$

where $P(b)$ is the reaction probability, $b_n = n \times d$ [$n = 0, 1, \ldots, n_{\max} = 7$], and d is 1 bohr.

D. Franck-Condon (FC) model

The Franck-Condon model[38,69–72] has recently been used for interpreting the rotational effects in bimolecular reactions.[40] Based on the premise of sudden collision, the FC model attributes the mode specificity to overlaps between reactant rotational states and transition-state wavefunctions in the angular domain. As discussed in our previous work,[40] the FC model is applicable to reactions where reactant rotations are uncoupled with the reaction coordinate at the transition state, such as in the title reaction. Such overlaps provide valuable information on the tightness of the angular coordinate at the transition state perpendicular to the reaction coordinate, which can be considered as a quantum mechanical analog of the cone of acceptance.[73]

To compute the FC overlaps for this reaction, the lowest-lying angular transition-state wavefunctions were first determined. To this end, fixing all radial coordinates at their values at the transition state transforms the 7D Hamiltonian in Eq. (1) to the following four-dimensional (4D) transition-state Hamiltonian:

$$\hat{H}^{TS} = \frac{(\hat{J}_{tot} - \hat{J})^2}{2\mu_R {R_{TS}}^2} + \frac{\hat{l}^2}{2\mu_r {r_{TS}}^2} + \hat{K}^{rot}_{CZ_3} + V(R_{TS}, r_{TS}, \chi_{TS}, \theta_1, \varphi_1, \theta_2, \varphi_2), \quad (26)$$

where R_{TS}, r_{TS}, and χ_{TS} are their corresponding values at the saddle point. Digonalizing this Hamiltonian yields four-dimensional angular wavefunctions at the transition state ($|\psi^{J_{tot}K_{tot}N}_{TS}(\theta_1, \varphi_1, \theta_2, \varphi_2)\rangle$), where N denotes collectively the bending quantum numbers. In the same spirit, one can calculate each rotational state $|\psi^{J_{tot}K_{tot}JK}_0(\theta_1, \varphi_1, \theta_2, \varphi_2)\rangle$ of CHD_3 based on the analogous Hamiltonian in the asymptote, where $R = R_\infty$, $r = r_{eq}$, and $\chi = \chi_{eq}$. The same CS approximation as in the QD calculations was used. Note that the rotational

wavefunctions for CHD_3, which is a symmetric top, essentially depend on (θ_1, φ_1) only. The overlaps between an initially rotational state and the transition-state wavefunctions are hence evaluated in (θ_1, φ_1) with (θ_2, φ_2) fixed at the transition-state values,

$$P_{J_{tot}K_{tot}JK} = \left|\psi_0^{J_{tot}K_{tot}JK}(\theta_1, \varphi_1, \theta_2, \varphi_2)\right| \times \psi_{TS}^{J_{tot}K_{tot}N}(\theta_1, \varphi_1, \theta_2, \varphi_2)\rangle. \quad (27)$$

In FC calculations, N is chosen as the lowest one, although higher ones can be used for higher energies.[74] It is interesting to note that there are selection rules dictated by the rotational matrices used to describe the overall rotation. As a result, the transition-state wavefunction used in computing the FC overlaps is not always the one with the lowest energy, but the lowest state with a non-zero overlap with a specific initial state.

III. RESULTS AND DISCUSSION

Figure 2(a) exemplifies the time-sliced raw images of the $CD_3(v = 0)$ products, excited via all four branches, at $E_c = 3.6$ kcal mol^{-1}. The raw images shown are from stretch-excited reaction only, for which the contributions of the residual ground-state reaction have been properly subtracted from the IR-on images.[11,13] From the concurrent measurement of the fraction of CHD_3 reactants being IR-excited and contributing to the observed product signals,[51] the relative reactivity of the rotationally state-selected Cl + $CHD_3(v_1 = 1, JK)$ reactions can be deduced through image analysis. The results are summarized in Fig. 2(b). In particular, the initial states are labeled by the rotational branches used in the IR excitation, and correspond to $J = 0$, $K = 0$; $J = 1$, $K = 0$; $J = 1$, $K = \pm 1$; and $J = 2$, $K = 0, \pm 1$ for $P(1)$, $R(0)$, $Q(1)$, and $R(1)$, respectively. Clearly, the initial rotation excitation of the reagents exerts a prominent, positive effect in promoting the reactivity. Specifically, the reactivity increase with J and lower K values yield higher reactivity within a J manifold. Similar rotational enhancement, albeit qualitatively, has also been observed in the reaction of Cl with CH_3D.[75] In view of the smallness of the rotational energy (merely $\sim$20 cm^{-1} for $J = 2$), such a profound enhancement in reactivity is quite remarkable. A slightly higher, albeit subtle, efficacy in rate-enhancement for $JK = 10$ than 1 ± 1 is noted.

While the experimental data are measured for the ground vibrational state of CD_3, all theoretical results presented below are summed over all product states,. However, preliminary QD calculations suggest that the ratios of probabilities for $v_2(CD_3) = 0$ and all CD_3 states are very close. In other words, the states of CD_3 are not expected to qualitatively change the rotational enhancement patterns discussed here.

Figure 3(a) displays the QD reaction probabilities for different JK states of $CHD_3(v_1 = 1)$. For $J = 0$, its projection on r (K) and the helicity quantum number K_{tot} are necessarily zero. For $J > 0$, the values of K and K_{tot} range from 0 to J. For each (J, K, K_{tot}) initial state, the quantum dynamics

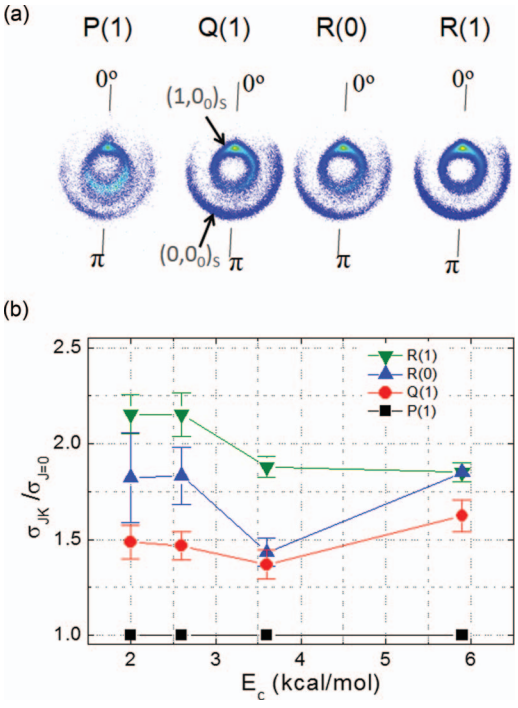

FIG. 2. (a) Raw images of the $CD_3(v = 0)$ products in the stretch-excited reactions, pumped via four rotational branches of the $CHD_3(v_1 = 1 \leftarrow 0)$ transition, are exemplified at $E_c = 3.6$ kcal mol^{-1}. Shown are the difference images between the recorded IR-on image and $(1 - n^{\neq}/n_0)$ IR-off image. (b) Dependency of relative reactivity on the rotational states of $CHD_3(v_1 = 1)$ reactants. At each E_c, the reactivity of the rotational ground state is set at unity.

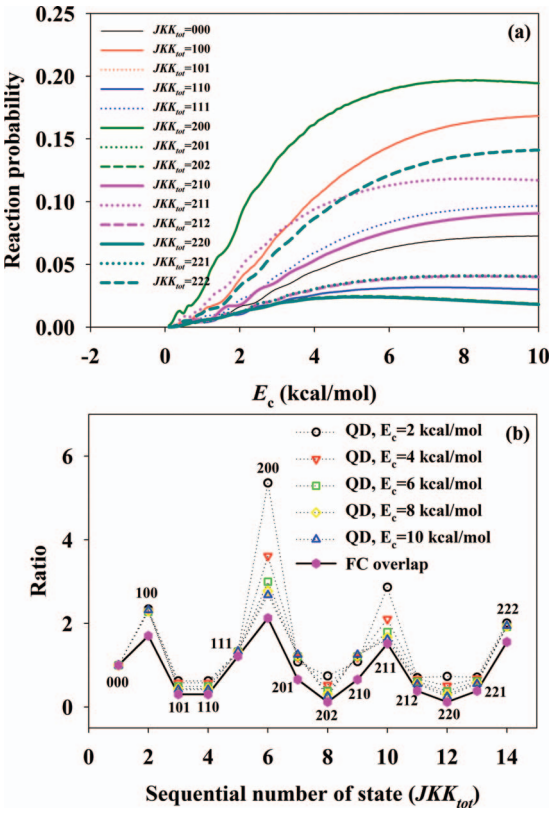

FIG. 3. (a) QD reaction probabilities for the Cl + $CHD_3(v_1 = 1, JK) \rightarrow$ HCl + CD_3 reaction from different initial rotational states as a function of collision energy. (b) Comparison of the FC values with the reaction probabilities at different collision energies.

calculation was carried out only with $J_{tot} = K_{tot}$ and J-shift approximation is employed for $J_{tot} > K_{tot}$ for the integral cross section calculations. It is clear that the reaction probabilities all increase with the collision energy, and there is essentially no reaction threshold, suggesting that a significant part of the reactant vibrational energy is used to overcome the classical reaction barrier (7.6 kcal/mol). This is consistent with the sudden vector projection (SVP) model, which suggests a strong coupling between the C–H stretching (v_1) mode of CHD_3 and the reaction coordinate at the transition state.[76] On the other hand, the SVP model predicts no enhancement for rotational excitation of CHD_3, as the rotational motions are poorly coupled with the reaction coordinate at the transition state.[76]

However, Fig. 3(a) clearly shows that the reactivity is different from different initial rotational states. To understand the mode specific behavior, we resort to the FC model. As discussed above, the FC model is based on the premise that the collision is sudden, and the reactivity is proportional to the overlap between a reactant quantum state wave function with the transition-state wave function near the saddle point, at least for energies near the reaction threshold. The transition-state wave functions are approximated by solving the bending problem at the transition state of the title reaction. The overlaps are collected in Table I for the lowest few rotational states of $CHD_3(v_1 = 1)$. As shown in Fig. 3(b), the ordering of the FC overlaps is generally consistent with the corresponding reaction probabilities at several collision energies. There are several additional interesting observations. First, the reaction probability increases with J for the $K = 0$ stack with $K_{tot} = 0$, which is apparently due to the improved overlap with the lowest transition-state wave function for low J states. As J increases further, the overlap starts to decay (data not shown), signaling inhibition. This has been seen in the $H + H_2$ reaction,[40] which also has a collinear transition state and H_2 rotation can be likened with the $J0$ states of CHD_3. Second, there is a strong propensity for $K = K_{tot}$, and the overlaps for (J,K,K_{tot}) and (J,K_{tot},K) states are the same, which is dictated by properties of the rotational matrix. An important fact corresponding to this behavior is that one needs to average various K_{tot} results when simulating the rotational effects on the cross sections. The overall good agreement validates the FC model, underscoring the importance of bending vibration at the transition state. Indeed, the enhancement observed here is related to the cone of acceptance[73] in reactions dominated by a collinear transition state, in which the coupling between the reactant rotation and reaction coordinate at the transition state is zero. Under such circumstances, the tightness of the saddle point in the angular coordinates dictates the flux passing through the transition state.

TABLE I. Franck-Condon overlaps between an initial state (J,K,K_{tot}) of CHD_3 and transition-state wave functions. The energy of each state is given in cm^{-1}.

(J,K,K_{tot})	Initial state	Transition state	Overlap
(0,0,0)	1222.3	3742.2	0.1246
(1,0,0)	1226.8	3742.2	0.2122
(1,0,1)	1226.8	3999.6	0.0379
(1,1,0)	1225.9	3998.6	0.0379
(1,1,1)	1225.9	3743.7	0.1513
(2,0,0)	1236.0	3742.2	0.2652
(2,0,1)	1236.0	3999.6	0.0820
(2,0,2)	1236.0	4284.2	0.0152
(2,2,0)	1232.2	4280.0	0.0153
(2,1,0)	1235.0	3743.7	0.0820
(2,2,1)	1232.2	4000.0	0.0482
(2,1,1)	1235.0	3743.7	0.1891
(2,2,2)	1232.2	3747.8	0.1939
(2,1,2)	1235.0	4003.7	0.0482

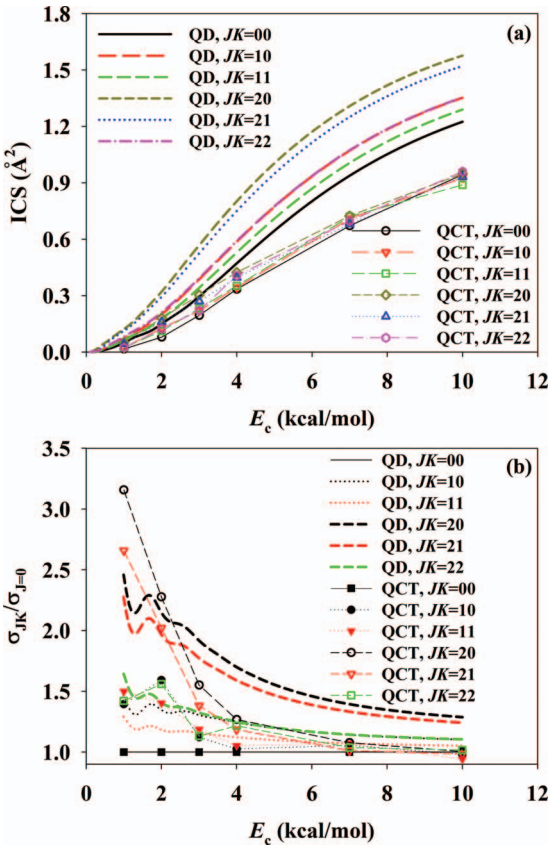

FIG. 4. (a) QD and QCT ICSs for the Cl + $CHD_3(v_1 = 1,JK)$ → HCl + CD_3 reactions as a function of the collision energy. (b) JK-dependence of the cross section ratios ($\sigma_{JK}/\sigma_{J=0}$) as a function of collision energy.

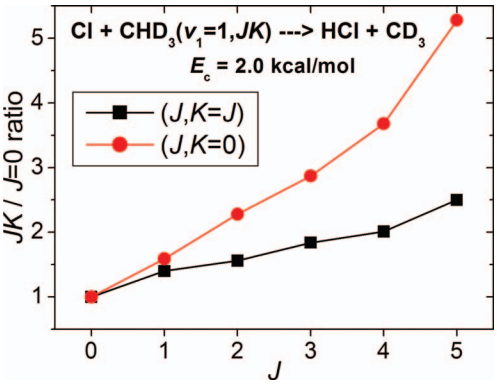

FIG. 5. K-dependence of the cross section ratios as a function of J at collision energy of 2.0 kcal/mol for the Cl + $CHD_3(v_1 = 1,JK)$ → HCl + CD_3 reactions.

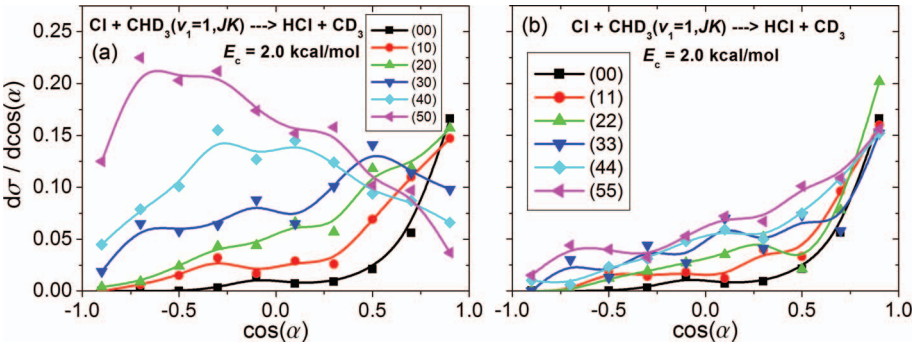

FIG. 6. Initial attack angle distributions at collision energy of 2.0 kcal/mol for the Cl + $CHD_3(v_1 = 1,JK) \rightarrow HCl + CD_3$ reactions with $K = 0$ (left) and $K = J$ (right). α is defined at $t = 0$ as the angle between the CH vector and the initial velocity vector of CHD_3.

In Fig. 4(a), the QD integral cross sections (ICSs) for the Cl + $CHD_3(v_1 = 1$, $JK = 00$, 10, 11, 20, 21, and 22) reaction are displayed as a function of the collision energy. It is clear that in all cases, the ICSs have no threshold and increase monotonically with E_c. This is consistent with the previous experimental threshold of less than 0.5 kcal/mol.[11] More importantly, the larger J values are typically more reactive, which is consistent with the experimental observations mentioned above. The dependence on K is more subtle, as indicated by Fig. 4(b) where the enhancement ratios ($\sigma_{JK}/\sigma_{J=0}$) are plotted. The QD ratios of the ICSs are consistent with the experimental data shown in Fig. 2(b), although the enhancement effects seem to diminish at higher collision energies.

To gain mechanistic insights into the rotational enhancement effects, we have computed the ICSs using a QCT method for the relevant CHD_3 ro-vibrational states, which are also included in Fig. 4(a). It appears that the QD-QCT agreement is better at low collision energies, but the latter are smaller than their QD counterparts at higher energies. The QCT $\sigma_{JK}/\sigma_{J=0}$ ratios for all JK states up to $J = 2$ are compared with the QD results in Fig. 4(b). These data are in rather good agreement with both the experimental and QD ratios at low energies, but the QCT enhancements diminish at high energies faster than the QD counterparts.

To better understand the K-dependence, we focus on the reaction dynamics of $CHD_3(v_1 = 1)$ rotational states up to $J = 5$ using the QCT approach. In Fig. 5, the $\sigma_{JK}/\sigma_{J=0}$ ratios are shown for $K = 0$ and $K = J$. The $J0$ states are significantly more reactive than the JJ states and the enhancement factors increase with increasing J. To understand this difference in reactivity, we plot in Fig. 6 the initial attack angle (α) distributions for reactive trajectories at $E_c = 2.0$ kcal/mol. The attack angle is defined at $t = 0$ as the angle between the CH vector and the initial velocity vector of CHD_3 and the distributions are averaged over impact parameters. At $J = 0$ a clear preference of α close to zero, which corresponds to the collinear Cl...H...CD_3 configuration if $b = 0$, is seen and almost no reactive events are found when Cl approaches CHD_3 from the back. This suggests that the initial orientation of the reactants is maintained while the reactants approach each other, consistent with a direct abstraction mechanism. Rotational excitation of $CHD_3(v_1 = 1)$ shifts the attack angle distributions toward larger α values especially for $K = 0$ states. For $JK = 50$ we see higher probability of H abstraction when the Cl initially approaches the CD_3 side of CHD_3. For $K = J$ states this effect is not seen, in this case the α distributions only slightly depend on J. These findings are consistent with α *vs.* impact parameter distributions shown in Fig. 7.

Attack angles as a function of the C–Cl distance for representative trajectories are shown in Fig. 8. For $J = 0$, α oscillates around a constant value while the reactants approach each other indicating little long-range stereo-chemical effects. Note that the oscillation is seen due to the bending motions of CHD_3. For $JK = 50$ the picture is quite different. The rotational motion (classically, a tumbling rotation) helps to decrease α and steers the reactants toward a reactive orientation. Nevertheless the average trajectory more or less follows a straight line (indicating again little long-range reorientation effects) with a slant slope (reflecting the rotational motion).

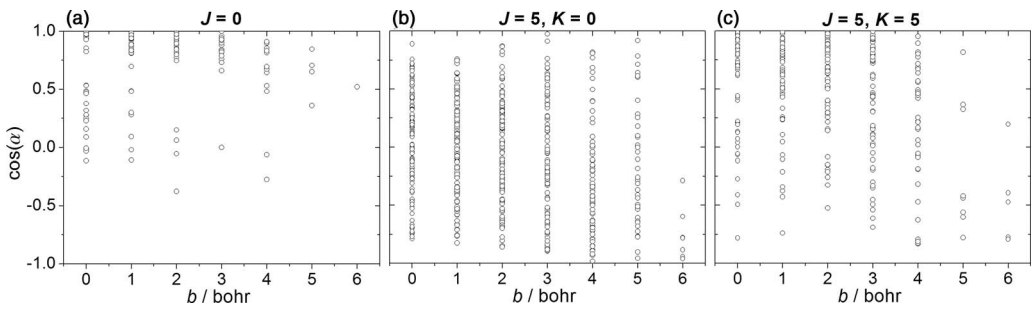

FIG. 7. Initial attack angle *vs.* impact parameter distributions at collision energy of 2.0 kcal/mol for the Cl + $CHD_3(v_1 = 1,JK) \rightarrow HCl + CD_3$ reactions with $JK = 00$ (left), 50 (middle), and 55 (right). α is defined at $t = 0$ as the angle between the CH vector and the initial velocity vector of CHD_3.

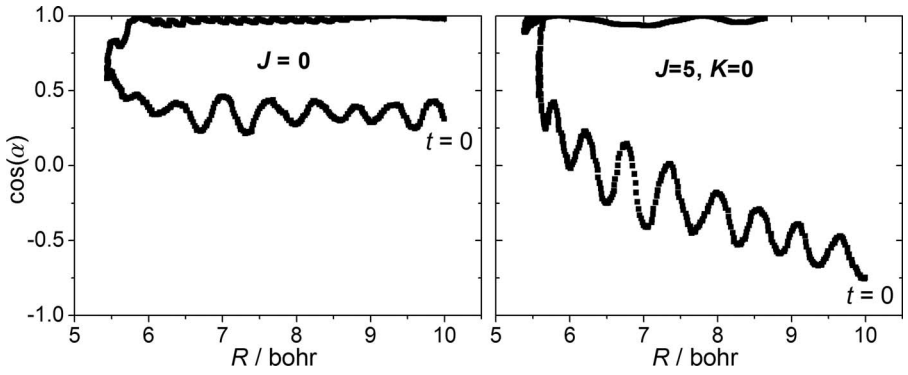

FIG. 8. Attack angle as a function of the C–Cl distance for representative Cl + $CHD_3(v_1 = 1,JK) \rightarrow HCl + CD_3$ trajectories with $JK = 00$ (left) and 50 (right). α is defined as the Cl-C-H angle and $b = 0$.

The conclusion of a weak long-range anisotropic interaction corroborates well with the enormous steric effects recently observed in the Cl + polarized-$CHD_3(v_1 = 1)$ studies;[47–50,77] otherwise, the initially selected alignment of the $CHD_3(v_1 = 1, JK = 10)$ reactants would have been scrambled by the long-range anisotropic forces. In every case the abstraction occurs at around 5.4 bohrs C–Cl distance, where α drops to zero. This is consistent with the C–Cl distance of 5.4 bohrs at the transition state.

The QCT results suggest that for $K = 0$ increasing the J value of the CHD_3 reactant up to 5 promotes the reaction by accessing a larger and larger cone of acceptance, consistent with the FC model. On the other hand, increasing the K value is less effective in promoting the reaction as the rotation with $J = K$ is essentially about the C–H axis (classically, a spinning rotation), which has no effect in opening the cone of acceptance. Indeed, the angle of attack for these states is very much like the $J = 0$ case, as seen in Fig. 6.

IV. CONCLUSIONS

In this work, we present experimental evidence for rotational mode specificity for a prototypical bimolecular reaction. Specifically, cross sections have been measured for the Cl + $CHD_3(v_1 = 1, JK) \rightarrow HCl + CD_3$ reaction and the low-lying rotational states of CHD_3 are found to be more reactive than its rotationless counterpart. The reaction dynamics is investigated using both a reduced-dimensional quantum mechanical model and quasi-classical trajectory method. Both reproduced the experimental observation qualitatively. The rotational enhancement effect was analyzed using both trajectories and a Franck-Condon model. It is found that the enhancement due to increasing J value of the reactant can be attributed to the opening of the cone of acceptance, while the increasing of K is much less effective as the energy is largely imparted into the rotation along the C–H bond. It should be emphasized that both experimental results and theoretical analysis are limited to the lowest few rotational states, and further rotational excitation might inhibit the reaction. Nevertheless, the detailed analysis presented in this work allows a better understanding of how reactant rotational excitation affects the reactivity in reactions involving polyatomic molecules.

ACKNOWLEDGMENTS

This work was supported by Academia Sinica and Minister of Science and Technology of Taiwan (MOST 102-2119-M-001 to K.L.), National Science Foundation of China (Grant No. 21322309 to F.W., and 21221064 and 21373266 to M.Y.), Scientific Research Fund of Hungary (OTKA, NK83583 to G.C.), and US Department of Energy (DE-FG02-05ER15694 to H.G.). F.W. and K.L. thank Dr. Y. Cheng and J.-S. Lin for assisting experiments.

[1] F. F. Crim, Acc. Chem. Res. **32**, 877 (1999).
[2] F. F. Crim, Faraday Discuss. **157**, 9 (2012).
[3] R. D. Beck and A. L. Utz, in *Dynamics of Gas-Surface Interactions*, edited by R. D. Muino and H. F. Busnengo (Springer, Heidelberg, 2013).
[4] R. N. Zare, Science **279**, 1875 (1998).
[5] J. C. Polanyi, Science **236**, 680 (1987).
[6] Z. H. Kim, H. A. Bechtel, and R. N. Zare, J. Am. Chem. Soc. **123**, 12714 (2001).
[7] S. Yoon, R. J. Holiday, E. L. Sibert III, and F. F. Crim, J. Chem. Phys. **119**, 9568 (2003).
[8] S. Yoon, R. J. Holiday, and F. F. Crim, J. Chem. Phys. **119**, 4755 (2003).
[9] H. A. Bechtel, J. P. Camden, D. J. A. Brown, and R. N. Zare, J. Chem. Phys. **120**, 5096 (2004).
[10] J. P. Camden, H. A. Bechtel, D. J. A. Brown, and R. N. Zare, J. Chem. Phys. **123**, 134301 (2005).
[11] S. Yan, Y. T. Wu, B. Zhang, X.-F. Yue, and K. Liu, Science **316**, 1723 (2007).
[12] W. Zhang, H. Kawamata, and K. Liu, Science **325**, 303 (2009).
[13] F. Wang, J.-S. Lin, Y. Cheng, and K. Liu, J. Phys. Chem. Lett. **4**, 323 (2013).
[14] G. C. Schatz, M. C. Colton, and J. L. Grant, J. Phys. Chem. **88**, 2971 (1984).
[15] D. H. Zhang and J. C. Light, J. Chem. Soc. Faraday Trans. **93**, 691 (1997).
[16] G. Czakó and J. M. Bowman, J. Am. Chem. Soc. **131**, 17534 (2009).
[17] G. Czakó and J. M. Bowman, Science **334**, 343 (2011).
[18] Z. Zhang, Y. Zhou, D. H. Zhang, G. Czakó, and J. M. Bowman, J. Phys. Chem. Lett. **3**, 3416 (2012).
[19] B. Fu and D. H. Zhang, J. Chem. Phys. **138**, 184308 (2013).
[20] J. Li, B. Jiang, and H. Guo, J. Am. Chem. Soc. **135**, 982 (2013).
[21] B. Jiang and H. Guo, J. Am. Chem. Soc. **135**, 15251 (2013).
[22] R. Liu, M. Yang, G. Czakó, J. M. Bowman, J. Li, and H. Guo, J. Phys. Chem. Lett. **3**, 3776 (2012).
[23] G. Czakó, R. Liu, M. Yang, J. M. Bowman, and H. Guo, J. Phys. Chem. A **117**, 6409 (2013).
[24] S. Yan, Y.-T. Wu, and K. Liu, Proc. Natl. Acad. Sci. U.S.A. **105**, 12667 (2008).
[25] B. Jiang and H. Guo, J. Chem. Phys. **138**, 234104 (2013).
[26] J. Zhang, D. X. Dai, C. Wang, S. Harich, X. Wang, X. Yang, M. Gustafasson, and R. T. Skodje, Phys. Rev. Lett. **96**, 093201 (2006).
[27] Y. Xu, B. Xiong, Y. C. Chang, and C. Y. Ng, J. Chem. Phys. **137**, 241101 (2012).
[28] Y. Xu, B. Xiong, Y. C. Chang, and C. Y. Ng, J. Chem. Phys. **139**, 024203 (2013).

[29]G. D. Barg, H. R. Mayne, and J. P. Toennies, J. Chem. Phys. **74**, 1017 (1981).
[30]F. J. Aoiz, V. J. Herrero, and V. Sáez Rábanos, J. Chem. Phys. **94**, 7991 (1991).
[31]F. J. Aoiz, H. K. Buchenau, V. J. Herrero, and V. Sáez Rábanos, J. Chem. Phys. **100**, 2789 (1994).
[32]F. J. Aoiz, L. Bañares, V. J. Herrero, G. Stark, and H. J. Werner, Chem. Phys. Lett. **254**, 341 (1996).
[33]D. H. Zhang and S.-Y. Lee, J. Chem. Phys. **109**, 2708 (1998).
[34]F. J. Aoiz, L. Bañares, J. F. Castillo, and V. J. Herrero, J. Chem. Phys. **111**, 9891 (1999).
[35]D. H. Zhang and S.-Y. Lee, J. Chem. Phys. **112**, 203 (2000).
[36]S. Sukiasyan and H. D. Meyer, J. Phys. Chem. A **105**, 2604 (2001).
[37]M. Hayes, M. P. Deskevich, D. J. Nesbitt, K. Takahashi, and R. T. Skodje, J. Phys. Chem. A **110**, 436 (2006).
[38]M. Gustafsson and R. T. Skodje, J. Chem. Phys. **124**, 144311 (2006).
[39]N. Bulut, J. Kłos, and M. H. Alexander, J. Chem. Phys. **136**, 104304 (2012).
[40]B. Jiang, J. Li, and H. Guo, J. Chem. Phys. **140**, 034112 (2014).
[41]B. Jiang, D. Xie, and H. Guo, J. Chem. Phys. **135**, 084112 (2011).
[42]J. Li and H. Guo, Chin. J. Chem. Phys. **26**, 627 (2013).
[43]A. Li, Y. Li, H. Guo, K.-C. Lau, Y. Xu, B. Xiong, Y.-C. Chang, and C. Y. Ng, J. Chem. Phys. **140**, 011102 (2014).
[44]H. Song, J. Li, B. Jiang, M. Yang, Y. Lu, and H. Guo, J. Chem. Phys. **140**, 084307 (2014).
[45]F. Meng, W. Yan, and D. Wang, Phys. Chem. Chem. Phys. **14**, 13656 (2012).
[46]J. Riedel, S. Yan, H. Kawamata, and K. Liu, Rev. Sci. Instrum. **79**, 033105 (2008).
[47]F. Wang, J.-S. Lin, and K. Liu, Science **331**, 900 (2011).
[48]F. Wang, K. Liu, and T. P. Rakitzis, Nat. Chem. **4**, 636 (2012).
[49]F. Wang and K. Liu, Chin. J. Chem. Phys. **26**, 705 (2013).
[50]F. Wang, J.-S. Lin, and K. Liu, J. Chem. Phys. **140**, 084202 (2014).
[51]Y. Cheng, H. Pan, F. Wang, and K. Liu, Phys. Chem. Chem. Phys. **16**, 444 (2014).
[52]J. G. Zhou, J. J. Lin, W. C. Shiu, S. C. Pu, and K. Liu, J. Chem. Phys. **119**, 2538 (2003).
[53]J. Zhou, W. Shiu, J. J. Lin, and K. Liu, J. Chem. Phys. **120**, 5863 (2004).
[54]J. Zhou, W. Shiu, J. J. Lin, and K. Liu, J. Chem. Phys. **124**, 104309 (2006).
[55]J. J. Lin, J. Zhou, W. Shiu, and K. Liu, Rev. Sci. Instrum. **74**, 2495 (2003).
[56]D. M. Sonnenfroh and K. Liu, Chem. Phys. Lett. **176**, 183 (1991).
[57]S. Yan, Y.-T. Wu, and K. Liu, Phys. Chem. Chem. Phys. **9**, 250 (2007).
[58]J. Palma and D. C. Clary, J. Chem. Phys. **112**, 1859 (2000).
[59]M. Yang, D. H. Zhang, and S.-Y. Lee, J. Chem. Phys. **117**, 9539 (2002).
[60]M. Yang, S.-Y. Lee, and D. H. Zhang, J. Chem. Phys. **126**, 064303 (2007).
[61]G. Czakó and J. M. Bowman, J. Chem. Phys. **136**, 044307 (2012).
[62]R. N. Zare, *Angular Momentum* (Wiley, New York, 1988).
[63]D. T. Colbert and W. H. Miller, J. Chem. Phys. **96**, 1982 (1992).
[64]J. A. Flect, Jr., J. R. Morris, and M. D. Feit, Appl. Phys. **10**, 129 (1976).
[65]R. T. Pack, J. Chem. Phys. **60**, 633 (1974).
[66]P. McGuire and D. J. Kouri, J. Chem. Phys. **60**, 2488 (1974).
[67]D. H. Zhang and J. Z. H. Zhang, J. Chem. Phys. **101**, 1146 (1994).
[68]W. L. Hase, in *Encyclopedia of Computational Chemistry*, edited by N. L. Alinger (Wiley, New York, 1998), Vol. **1**, pp. 399–402.
[69]M. J. Berry, Chem. Phys. Lett. **27**, 73 (1974).
[70]G. C. Schatz and J. Ross, J. Chem. Phys. **66**, 1021 (1977).
[71]D. Wang and J. M. Bowman, Chem. Phys. Lett. **207**, 227 (1993).
[72]R. Welsch and U. Manthe, Mol. Phys. **110**, 703 (2012).
[73]R. D. Levine, J. Phys. Chem. **94**, 8872 (1990).
[74]D. Wang and J. M. Bowman, J. Phys. Chem. **98**, 7994 (1994).
[75]A. E. Berke, E. H. Volpa, C. J. Annesley, and F. F. Crim, J. Chem. Phys. **138**, 224306 (2013).
[76]B. Jiang and H. Guo, "Mode Specificity, Bond Selectivity, and Product Energy Disposal in X + CH_4/CHD_3 (X=H, F, O(^{3}P), Cl, and OH) Hydrogen Abstraction Reactions: Perspective from Sudden Vector Projection Model," J. Chin. Chem. Soc. (published online).
[77]W. R. Simpson, T. P. Rakitzis, S. A. Kandel, A. J. Orr-Ewing, and R. N. Zare, J. Chem. Phys. **103**, 7313 (1995).